Acta Crystallographica Section D
Biological Crystallography
ISSN 0907-4449

Metals in the sporulation phosphorelay: manganese binding by the response regulator Spo0F

Debashis Mukhopadhyay,‡ Udayaditya Sen,‡ James Zapf and Kottayil I. Varughese*

Division of Cellular Biology, Department of Molecular and Experimental Medicine, The Scripps Research Institute, La Jolla, CA 92037, USA

‡ These authors made equal contributions.

Correspondence e-mail: kiv@scripps.edu

Received 7 October 2003
Accepted 27 January 2004

PDB Reference: metal-bound Spo0F, 1pey, r1peysf.

As a part of studies on the structural characterization of the components of the sporulation phosphorelay in *Bacillus subtilis*, the crystal structure of the manganese derivative of an intermediate signal transducer, Spo0F, has been elucidated at 2.25 Å resolution. The calcium complex and the apo structures have been analyzed previously. In apo Spo0F, the active-site cation cavity is only partially formed and it only becomes completed upon metal coordination. The carbonyl of Lys56 is coordinated to the metal and interestingly the side chain of Lys56 exists in a variety of conformations in the three crystal structures of Spo0F. The affinity of the magnesium ion for Spo0F is in fact low; however, it binds Spo0F when it is in complex with Spo0B. It is proposed that the existence of a deep pocket which extends from the surface to the metal site could attract and direct the metal, thereby facilitating the metal binding of the complex.

1. Introduction

The transfer of a phosphoryl group from one protein to another is the basis of signal propagation in most regulatory pathways in the cell. Bacterial adaptations make use of 'two-component systems' that transfer the phosphoryl group from the histidine kinases to the response regulators. Sporulation in *Bacillus subtilis* is controlled by a phosphorelay that is an expanded version of the two-component system (Burbulys *et al.*, 1991). In this phosphorelay, the flow of phosphate is from a histidine kinase to Spo0F (a secondary messenger) to Spo0B (the phosphotransferase) and then to Spo0A (the transcription factor). The process of phosphotransfer requires the coordination of a metal ion in the active site. The metal required for phosphotransfer is acquired and presented at the catalysis site by the response regulators Spo0F or Spo0A. Neither Spo0B nor histidine kinases possess any cation-binding sites (Grimshaw *et al.*, 1998).

Investigations into the metal centers in regulatory proteins are slowly revealing the expanding role of metals in modulating and fine-tuning the functions of proteins by utilizing their rich variety of coordination geometries and ligand-exchange rates (Dudev & Lim, 2003). Metals, particularly transition-metal ions, provide greater catalytic diversity (O'Halloran, 1993) to the enzymes. The roles of Ca^{2+}, Mg^{2+} or Fe^{2+} in living systems have been extensively studied during the last couple of decades mostly because of their high natural abundance (Holm *et al.*, 1996). During this period the metallobiochemistry of transition metals, particularly that of Mn^{2+}, has emerged as a substitute probe for the more abundant metals (Yocum & Pecoraro, 1999). As Mn^{2+} is paramagnetic in nature and has very nearly the same size as Mg^{2+}, the former was expected to be a good replacement for the latter in *in vitro*

Table 1
Some physicochemical properties of Mg^{2+}, Ca^{2+} and Mn^{2+} adopted from Cowan (1995).

Ion	Average ionic radius (Å)	Charge-to-radius ratio	Average ligand-exchange rate, k_{ex} (s^{-1})	Coordination No.	Geometry	Ligand preference
Mg^{2+}	0.86	2.33	5×10^5	6	Octahedral	O
Ca^{2+}	1.06	1.75	8×10^8	6–8	Flexible	O
Mn^{2+}	0.89	2.07	2×10^7	6	Octahedral	O, N

studies, especially in spectroscopic analysis (see Table 1 for detailed physico-chemical comparison; Cowan, 1995).

There are, however, certain subtle chemical differences between the two. In theory, manganese possesses a versatile range of oxidation states (−III to +VII) of which a wide range (+II to +VII) is found in living systems, as opposed to only one (+II) in the case of magnesium (Siegbahn, 2002). Mg^{2+} is a 'hard' cation preferring 'hard' ligands of low polarizability, whereas Mn^{2+} is a 'softer' cation having affinity for both oxygen and nitrogen. Additionally, Mn^{2+} has a more flexible coordination sphere and is more polarizable. Ca^{2+}, on the other hand, belongs to the 'harder' group of cations, preferring oxygen over nitrogen for binding in its single oxidation state (II). Mg^{2+} is rarely observed to bind to carboxylates in a bidentate fashion and it cannot replace Mn^{2+} or Ca^{2+} from their specific binding sites, but the reverse is generally true (Bock *et al.*, 1999; Dudev *et al.*, 1999; Dudev & Lim, 2001).

In *B. subtilis* Mn^{2+} is known to play a physiological role. For example, the involvement of Mn^{2+} ions in the sporulation of *B. subtilis* has long been reported (Charney *et al.*, 1951; Gould, 1969). However, its requirement as an essential element for sporulation was only realised after the understanding of manganese homeostasis (Que & Helmann, 2000). *B. subtilis* contains at least four distinct metal ion-dependent regulators, including MntR which is specific for manganese homeostasis. In addition to its roles in various responses and free-radical scavenging, its requirement in various stages of the *Bacillus* life-cycle, including spore formation and germination, has been reported (Horsburgh *et al.*, 2002; Jakubovics & Jenkinson, 2001). Inaoka *et al.* (1999) showed that the sporulation frequency decreases remarkably in superoxide dismutase-deficient bacilli under Mn^{2+}-depleted growth conditions. In *B. subtilis*, the physiological concentration of Mg^{2+} is of the order of 1 m*M*, which is low considering the K_d of 20 m*M* for Spo0F. Hence, we were intrigued by the following question: does the phosphorelay use other biologically relevant metals such as Mn^{2+} or Ca^{2+} which have higher affinity for Spo0F or does the association of Spo0F with KinA or Spo0B create a higher affinity environment for Mg^{2+}?

With the goal of elucidating the mechanism of signal propagation, the structures of Spo0F (Madhusudan *et al.*, 1996, 1997), Spo0B (Varughese *et al.*, 1998), the complex of Spo0F with Spo0B (Zapf *et al.*, 2000) and the effector domain of the transcription factor in complex with the target DNA (Zhao *et al.*, 2002) have been analyzed in our laboratory. The active site of Spo0F contains an acidic cluster that serves as a binding pocket for cations. Although the presence of cations in phosphotransfer proteins is not uncommon, introduction of a cation to Spo0F drew attention as it caused rearrangements in the active site to create a cation-binding site (Madhusudan *et al.*, 1996, 1997).

Table 2
Affinity of Spo0F Y13W mutant to different metals in comparison with other response regulators (Lukat *et al.*, 1990; Guillet *et al.*, 2002).

Cation	K_d (m*M*) Spo0F, pH 7	CheY†	DivK, pH 8
Ca^{2+}	3.5	6.1	—
Mg^{2+}	20	0.5	47
Mn^{2+}	2.5	0.05	1.34

† For CheY, Mg^{2+} and Mn^{2+} affinities were estimated at pH 7.0 and that for Ca^{2+} at pH 7.4.

In biological processes metals play diverse roles: they take part in connecting distant residues, serve as a mediator in protein–ligand interactions and act as a nucleophilic catalyst or an electron-transfer agent. In phosphoryl-transfer reactions, cations play a crucial role by reducing repulsive forces and by polarizing the P—O bond (Knowles, 1980; Lukat *et al.*, 1990; Zapf *et al.*, 2000).

Other response-regulatory proteins such as CheY or DivK (Guillet *et al.*, 2002; Lukat *et al.*, 1990) were found to bind various divalent cations with different affinities; Spo0F also follows the same pattern of cation binding (see Table 2). So far, crystal structures of only a few response regulators have been solved in complex with metal ligands: CheY with Mn^{2+} and Mg^{2+} (Lee *et al.*, 2001; Stock *et al.*, 1993), Rcp1 with Mn^{2+} (Im *et al.*, 2002), DivK with Mn^{2+} and Mg^{2+} (Guillet *et al.*, 2002), PhoP with Mn^{2+} (Birck *et al.*, 2003), Spo0A with Ca^{2+} (Lewis *et al.*, 1999) and Spo0F with Ca^{2+} and Mg^{2+} (Madhusudan *et al.*, 1997; Zapf *et al.*, 2000). In this paper, we present the structure of Spo0F Y13S mutant liganded to Mn^{2+} ion, which binds the protein with an octahedral coordination geometry. Additionally, regarding the possibility of phosphorelay using the low-affinity cation magnesium, we speculate on a possible mechanism of cation incorporation to the active site when Spo0F is in complex with its partner Spo0B.

2. Materials and methods

2.1. Protein expression and purification

B. subtilis Spo0F Y13S and Y13W mutants were overexpressed in *Escherichia coli* and purified by standard procedures (Burbulys *et al.*, 1991; Zapf *et al.*, 1996). The Y13S mutant form was chosen because it crystallizes more readily than the wild-type protein. The Y13W mutant was also produced for fluorescence studies. Our previous studies have shown that residue 13 is not involved in phosphotransfer and that mutation of this residue does not change the structure of the protein (Madhusudan *et al.*, 1996; Zapf *et al.*, 2000).

The sample was crystallized by the hanging-drop vapor-diffusion method using a 1:1 solution of the protein (at a concentration of ∼39 mg ml^{-1}) with 6% PEG 3350, 10%

Table 3
Data-collection and refinement statistics.

Values in parentheses refer to the highest resolution shell (2.29–2.25 Å).

Space group	$P4_32_12$
Unit-cell parameters (Å, °)	$a = b = 103.13$, $c = 83.64$, $\alpha = \beta = \gamma = 90.0°$
Redundancy	6.6
Maximum resolution (Å)	2.25
No. measured reflections	144584
No. unique reflections	21924 (1044)
Total completeness (%)	100.0 (100.0)
R_{sym} (%)	5.5 (66.8)
$I/\sigma(I)$	32.5 (2.0)
Refinement resolution range (Å)	50.0–2.25
No. reflections used in refinement	19808
R factor (%)	22.52
No. reflections used in R_{free}	1013
R_{free} (%)	25.76
R.m.s.d. from ideal bond lengths (Å)	0.008
R.m.s.d. from ideal bond angles (°)	1.8

glycerol and 100 m*M* $MnCl_2$ in 100 m*M* acetate buffer pH 4.5 equilibrated against 1 ml reservoir solution containing 7.5% PEG 3350, 10% glycerol, 200 m*M* $MnCl_2$ in the same buffer. Rod-like crystals appear after 2–3 d at 277 K, reaching maximum size after 7 d. The 100 m*M* concentration of $MnCl_2$ was crucial, as even slightly lower concentrations gave larger but poorly diffracting crystals. $MnCl_2$ was used as a source of divalent cations for phosphorylation as it was shown by fluorescence studies that Mn^{2+} has better binding ability than Mg^{2+} at the acidic binding pocket. The cryoprotectant solution standardized for Spo0F Y13S comprised 25% PEG 300 and 25% glycerol in 75 m*M* acetate buffer pH 4.5.

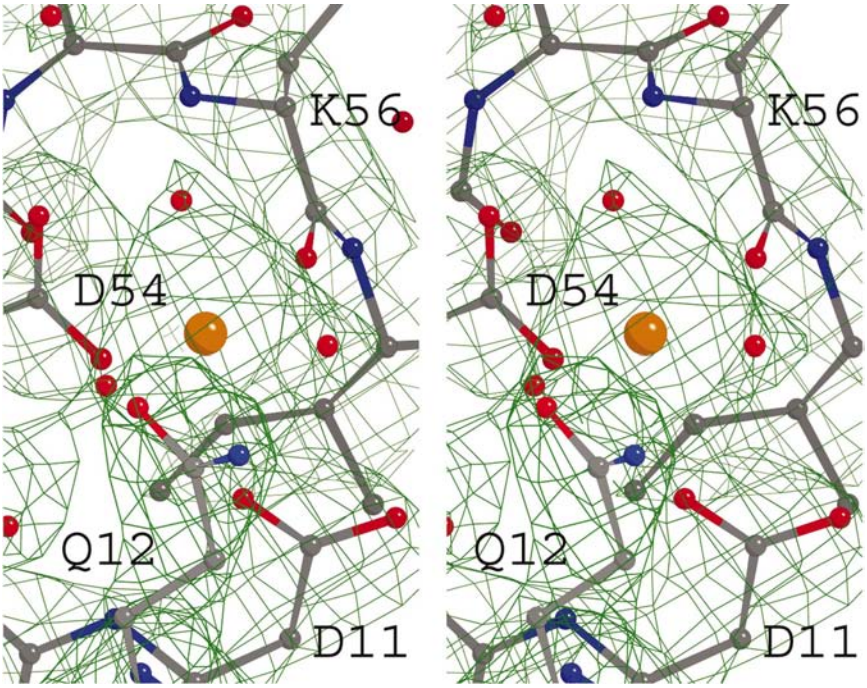

Figure 1
A $2|F_o| - |F_c|$ electron-density map (contoured at $\sim 1.5\sigma$) superimposed on the refined model, showing the Mn atom (orange) seated securely inside the catalytic pocket of molecule *B*. Important residues in the near vicinity are labeled.

2.2. Measurement of metal affinity by fluorescence quenching

Quenching experiments were performed with 2 µ*M* Spo0F Y13W mutant in 50 m*M* HEPES pH 7.0 and 250 m*M* KCl employing 1.0 *M* $MgCl_2$, $CaCl_2$ or $MnCl_2$ or 3.0 *M* KCl as ligands. Titrations were carried out and the data analyzed as described in Madhusudan *et al.* (1997).

2.3. Data collection

The data were collected using an in-house RU-200 rotating-anode X-ray generator and an R-AXIS IV^{++} image plate; all the crystals were tetragonal, belonging to space group $P4_32_12$. The crystal being studied was soaked in a cryosolution and frozen. It diffracted to 2.25 Å resolution and a total of 145 images were collected with 1° rotation and 600 s exposure per frame. The unit-cell parameters were $a = b = 103.12$, $c = 83.64$ Å, $\alpha = \beta = \gamma = 90°$. The data were processed using the programs *DENZO* and *SCALEPACK* (Gewirth, 1994; Otwinowski & Minor, 1997). The statistics for data-collection and refinement are compiled in Table 3.

2.4. Phasing and structural refinement

Even though there were variations between the unit-cell parameters (Table 3) of the present structure and the Ca^{2+}-bound crystal (Madhusudan *et al.*, 1996), the initial phasing attempt using the coordinates of the Ca^{2+} complex was successful. Refinements were carried out using the program *CNS* v.1.0. (Brünger *et al.*, 1998). All solvent molecules were excluded from the initial model. The *R* factor fell from 38.8 to 27.7% in successive steps of rigid-body refinement. The model was then refined by several rounds of torsional dynamics simulated annealing using a maximum-likelihood function, followed by anisotropic *B*-factor refinement with bulk-solvent correction. Manual adjustments to the model were performed using the program *O* v.7.0 (Jones *et al.*, 1991) based on an unbiased σ_A-weighted $2|F_o| - |F_c|$ map (Fig. 1), giving special attention to those residues in flexible loop regions and around the active-site groove as well as to the positions of metal atoms. Throughout the refinement, cross-validation of data using 5% (Brünger *et al.*, 1998) of the reflections and verification of atom positions by calculating omit maps were used to reduce bias towards the starting model. Solvent positioning, with density higher than 3.0σ, was performed only in the later stages of refinement. The electron densities for the metal ligands were the three highest positive peaks ($\sigma > 6.0$) in the $|F_o| - |F_c|$ σ_A-weighted map.

Spo0F models consisted of 119 (3–121) residues for molecule *A*, 120 (3–122) for molecule *B* and 120 (2–121) for molecule *C*.

Table 4
Bonding distances of metal ions from Spo0F active-site residues.

Cations	Residue atoms	Coordination distances (Å)		
		Mol. *A*	Mol. *B*	Mol. *C*
Mn^{2+}	Asp11 O2	2.17	2.39	2.38
	Asp54 O2	2.14	2.13	2.43
	Lys56 O	2.34	2.13	2.56
	Water O	2.25, 2.31, 2.59	2.11, 2.27, 2.31	2.28, 2.40
Ca^{2+}	Asp11 O1	2.05		2.04
	Asp54 O2	2.33		2.46
	Lys56 O	2.25		2.51
	Water O	2.1, 2.44	—	2.5

The final model additionally contains 183 ordered water molecules and the three Mn^{2+} ions. The final crystallographic *R* factor is 22.52% (R_{free} = 25.76%) for all reflections between 45 and 2.25 Å; all residues are in the allowed regions of a Ramachandran plot and more than 90% of them have the most favored backbone (φ, ψ) angles, as verified by *PROCHECK* (Laskowski *et al.*, 1993) and *WHAT-CHECK* (Hooft *et al.*, 1996). The average *B* factors are 43.7 $Å^2$ for main-chain atoms, 49.8 $Å^2$ for side-chain atoms and 51.0 $Å^2$ for all solvent atoms. The overall *B* factor from the Wilson plot is 50.0 $Å^2$. All the refinement protocols were carried out using *CNS* v.1.0 (Brünger *et al.*, 1998). The coordinate error of the model estimated from a Luzzati plot (Luzzati, 1952) is 0.4 Å.

3. Results

3.1. Overall description of the crystallographic model

Spo0F is a single-domain protein with an $(\alpha/\beta)_5$ fold. The overall structure is very similar to CheY and the N-terminal receiver domains of response regulators in the two-component/phosphorelay systems. The present crystal structure has three molecules of Spo0F per asymmetric unit as in the calcium complex (Madhusudan *et al.*, 1996). The protomer *A* is close to the crystallographic twofold axis and therefore is in proximity to a symmetrically related molecule, whereas protomers *B* and *C* are distant from the twofold axis and are positioned close to each other in the crystal lattice. All three molecules have very similar conformation and bind the cation in a nearly identical manner. The r.m.s. deviations arising on pairwise superposition of the individual protomers onto each other are all less than 0.6 Å. The electron-density distribution in the neighborhood of Mn^{2+} is shown in Fig. 1.

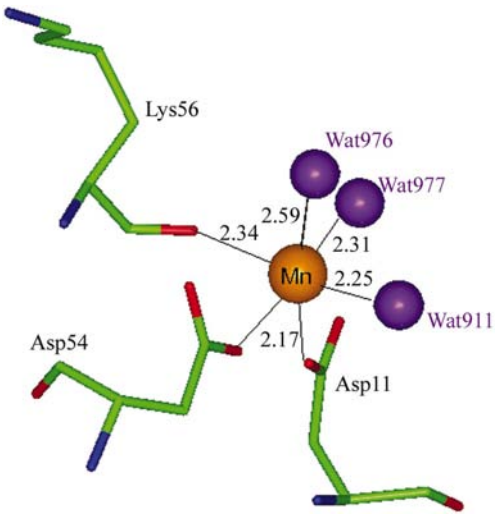

Figure 2
A cartoon showing the coordination of manganese with Spo0F. The water O atoms are colored purple for clarity. $Mn^{2+}\cdots O$ coordination distances (Å) are marked.

3.2. Interaction of Spo0F with metal ions

The geometry of coordination of Mn^{2+} is octahedral and is shown in Fig. 2. The cation binds to three O atoms of the protein and three water molecules. The Mn^{2+} ion is liganded to the main-chain carbonyl O atom of Lys56 with an average distance of 2.34 Å, to the carboxylates $O^{\delta 2}$ of Asp54 with an average distance of 2.23 Å and to Asp11 $O^{\delta 2}$ with an average distance of 2.31 Å. Additionally, Mn^{2+} is coordinated to three water O atoms in molecules *A* and *B*. The coordination geometry is octahedral as generally observed for divalent manganese. In molecule *C*, however, Mn^{2+} is coordinated only to two water molecules (see Table 4), giving a non-canonical distorted octahedral geometry.

When the affinities of the protein for divalent cations were measured by fluorescence quenching, a significant drop in intensity from the single engineered tryptophan at position 13 could be recorded. Like CheY and DivK (Lukat *et al.*, 1990; Guillet *et al.*, 2002) Spo0F also exhibits approximately tenfold less affinity for Mg^{2+}. Mn^{2+} and Ca^{2+} bind Spo0F with comparable affinities (Table 2).

3.3. Differences from the apo structure and the calcium-bound structure

The overall structure of the Mn^{2+}-bound Spo0F is similar to that of the apo molecule. The C^{α} superposition of molecules *A*, *B* and *C* with the apo structure gave r.m.s.d.s of 0.87, 1.04 and 0.92 Å, respectively. The metal-induced changes are mostly local and confined to the loop residues in the vicinity of the coordination site. The most drastic change upon metal coordination is in the orientation of the Asp11 side chain. This side chain, which pointed away from the active site in the metal-free structure, turns towards the metal for coordination. The other main differences are in the $\beta3$–$\alpha3$ and $\beta4$–$\alpha4$ loops. Both these loops exhibit displacements of about 3 Å for the main-chain atoms. In the $\beta3$–$\alpha3$ loop, the maximum movement is seen for the C^{α} of Pro58, which is shifted between 3.0 and 3.4 Å relative to the wild-type structure. Similarly, in the $\beta4$–$\alpha4$ loop, Tyr84 C^{α} moves between 3.0 and 3.5 Å. The $\beta3$–$\beta3$ loop is a tight γ-turn and in all three molecules it displays a uniform upward shift towards the $\beta4$–$\alpha4$ loop (Fig. 3). The flexible Lys56 side chains move away from the active-site pocket towards the $\beta4$–$\alpha4$ loop. Molecule *C* shows the minimum displacement for Lys56 side chain and interestingly one of the three coordinating water molecules is absent for this molecule.

In the present structure, all three molecules in the asymmetric unit are bound to metals, while in the calcium complex only molecules *A* and *C* are metal-coordinated. In both these cases, although the geometry is octahedral, Ca^{2+} is only coordinated to five O atoms. In the present crystal structure, Mn^{2+} is coordinated to six O atoms in molecules *A* and *B*, while in molecule *C* it is pentacoordinate. Lys56 is located in the vicinity of the active site and its carbonyl ligates the cation. In the present Mn^{2+}-bound structure, the side chains of Lys56 in all three monomers are well defined and oriented away from the metal site. By contrast, in the Ca^{2+}-bound structure the side chains of Lys56 are disordered in monomers *B* and *C*.

3.4. Comparison to other metal-bound response-regulator structures

Bellsolell *et al.* (1994) reported the structure of a CheY–Mg^{2+} complex crystallized in the presence of 200 m*M* magnesium acetate and showed large conformational changes upon metal binding. In addition to the reorientation of the active-site residues Asp57, Asp13, Asp12 and Lys109, this structure exhibited significant movement of the $\beta5$–$\alpha5$ loop, the formation of a new β-turn in the $\beta4$–$\alpha4$ loop and intrinsic instability of the $\alpha4$ helix. In contrast, another CheY–Mg^{2+} crystal structure determined in the presence of 10 m*M* $MgCl_2$ (Stock *et al.*, 1993) showed metal-induced perturbations to be located close to the active site only. The larger conformational changes seen in the structure of Bellsolell and coworkers was attributed to the high salt concentration. Although the Spo0F–Mn^{2+} complex was crystallized in the presence of 100 m*M* $MnCl_2$, the structural changes are moderate and are mostly localized.

Crystal structures of phosphorylated receiver domains of Spo0A (Lewis *et al.*, 1999) and FixJ (Li & Plamann, 1996) show that phosphorylation causes a drastic change in the $\beta4$–$\alpha4$ loop, reorienting a threonine residue (the equivalent of Thr82 in Spo0F) towards the active site. The movements resulting from metal coordination here are smaller than those observed for the phosphorylated states. Using NMR techniques, Gardino and coworkers have shown that when Spo0F interacts with BeF_3^-, which could mimic phosphorylation (Gardino *et al.*, 2003), the helix $\alpha1$ is displaced by half a turn downwards and the helices $\alpha3$ and $\alpha4$ show upward displacement by half a turn. All these observations shed light on the possible conformational changes upon metal binding and phosphorylation.

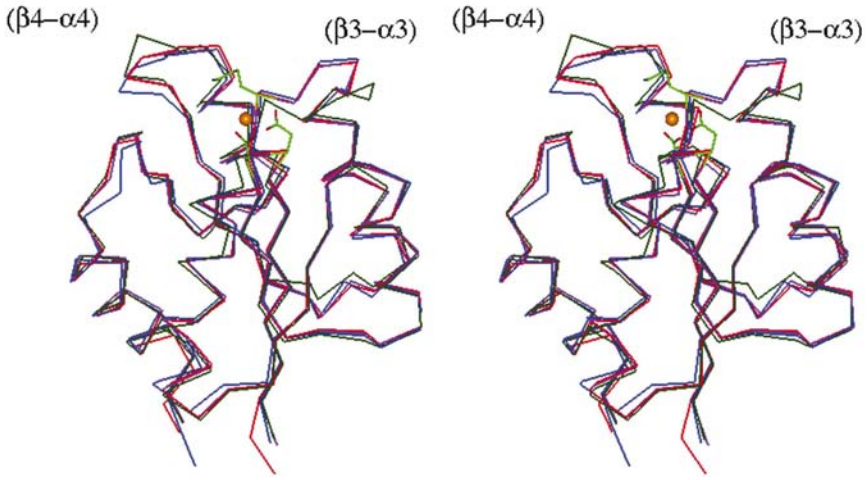

Figure 3
A C^{α}-trace superposition of the three molecules, *A* (purple), *B* (blue) and *C* (red), respectively, of Spo0F–Mn^{2+} with the wild-type model (in green) to show the upward movement of the two loops $\beta3$–$\alpha3$ and $\beta4$–$\alpha4$, narrowing the opening of the catalytic pocket in the metal complex. Catalytic residues Asp54, Asp11, Lys56 and the metal ion in Spo0F–Mn^{2+} are shown.

4. Discussion

Lukat *et al.* (1990) showed that divalent metal ions are required for transfer of phosphate from CheA to CheY and also for dephosphorylation of CheY. CheY is a single-domain response regulator like Spo0F. The binding affinities of CheY for several metals with varying charges and sizes have been studied (Needham *et al.*, 1993). The CheY binding site excludes monovalent cations, but binds divalent and trivalent cations. Spo0F binds Ca^{2+} and Mn^{2+} six and eight times tighter, respectively, than Mg^{2+} (Table 2).

4.1. Spo0F–Spo0B complex and a deep pocket

In the Spo0F–Spo0B complex (Zapf *et al.*, 2000), an Mg^{2+} ion is located in the same cation site as seen in the present structure and other cation-bound response regulators. One interesting aspect of the complex formation is that the cation sits at the bottom of a pocket about 11 Å deep. The mouth of the pocket is about 12 Å wide, but it narrows to about 6 Å at the bottom. In the vicinity of the mouth, there are several acid groups (*e.g.* Asp11, Glu86, Glu64 and Glu92 of Spo0F, and Asp14, Glu20 and Asp31 of Spo0B) (Fig. 4*a*). We suggest that the negative charges in the mouth could attract metals and channel them to the required site for catalysis. When the cations start moving into the pocket, the electrostatic forces will become more effective as the effective dielectric constant is lower in the partially buried environment (Shan & Herschlag, 1996).

The formation of the deep pocket may be considered to be the mechanism devised by nature to shield the phosphoaspartate from nucleophilic attack of water from outside (Goudreau *et al.*, 1998; Zapf *et al.*, 2000) and to stabilize the transition state. This in turn may create a microenvironment in which a particular cation may be chosen over another, catering to the specific rate of catalysis as demanded by the reaction pathway.

Thermodynamic studies on metal binding by Bock *et al.* (1999) showed that Mn^{2+} binds water and carboxylates less strongly than Mg^{2+}. Manganese, however, has an enhanced affinity towards nitrogen and

several N-containing groups, His30, His23, His27 and Asn34 from Spo0B, and Lys56, Gln12 and Lys104 from Spo0F, are situated either along the channel or close to the binding site (Fig. 4*b*). Once inside the groove, Mn^{2+} would therefore have a selective advantage over the other metals in being lured to the binding site. The possible competitive binding of Mn^{2+} with respect to Mg^{2+} in the complex *in vivo* is yet to be ascertained. Additionally, the inner-sphere water in Mn^{2+} complexes are more readily replaced by other groups than those of Mg^{2+} (Table 1). These properties and the higher binding affinity of Mn^{2+} for Spo0F make manganese a suitable candidate for binding to Spo0F either in the free form or when in complex with Spo0B.

4.2. A possible role for Lys56 in metal coordination and phosphoryl transfer

Enzymes discriminate against Mg^{2+} in favor of Mn^{2+} by inserting a nitrogen-containing ligand near the site of phosphorylation, as seen in *E. coli* phosphoenolpyruvate carboxykinase (PCK; Matte *et al.*, 1998; Tari *et al.*, 1997). In the PCK structure, Mn^{2+} is chelated by the alkylamine of a Lys residue, whereas Mg^{2+} binds in an all-oxygen environment. The lysine side chain which binds to Mn^{2+} has a lower pK_a value as it is surrounded by positively charged residues and is deprotonated (Tari *et al.*, 1997). In the metal-binding studies with DivK (Guillet *et al.*, 2002), an increased affinity for Mn^{2+} is reported at higher pH values owing to the deprotonation of a Cys thiol group in the vicinity. In the present structure, no visible structural rationale is seen for the tighter binding of Mn^{2+} than Mg^{2+} to Spo0F. However, we have previously shown that Lys56 has a role in regulating the Spo0F-P autophosphatase activity of Spo0F (Zapf *et al.*, 1998). It is conceivable that Lys56 could have a role in favoring Mn^{2+} coordination since Mn^{2+} is known to coordinate nitrogen and sulfur in addition to oxygen ligands, whereas Mg^{2+} strictly coordinates oxygen ligands. Provided that the alkylamine is deprotonated, the side chain of Lys56 is suitably positioned to coordinate Mn^{2+}.

We cannot make any clear conclusions about the involvement of Lys56 N^{ζ} in preferentially promoting Mn^{2+} binding as it is protonated at the pH values used to crystallize the protein. However, a comparison of the side-chain positions (Fig. 5) in the three crystal structures of Spo0F is interesting. In the metal-free structure, Lys56 N^{ζ} is closest to the location where the metal binds. Alternatively, the reason for the enhanced affinity of Mn^{2+} over Mg^{2+} may arise from the greater ease with which water is displaced by oxygen ligands such as those seen in the Spo0F structure. These properties and the higher affinity of Mn^{2+} could make manganese a suitable candidate for binding to Spo0F and catalyzing the phosphotransfer reactions.

5. Conclusion

A comparison of the structure of Mn^{2+} derivative of Spo0F with the calcium-bound and native structure gives us different

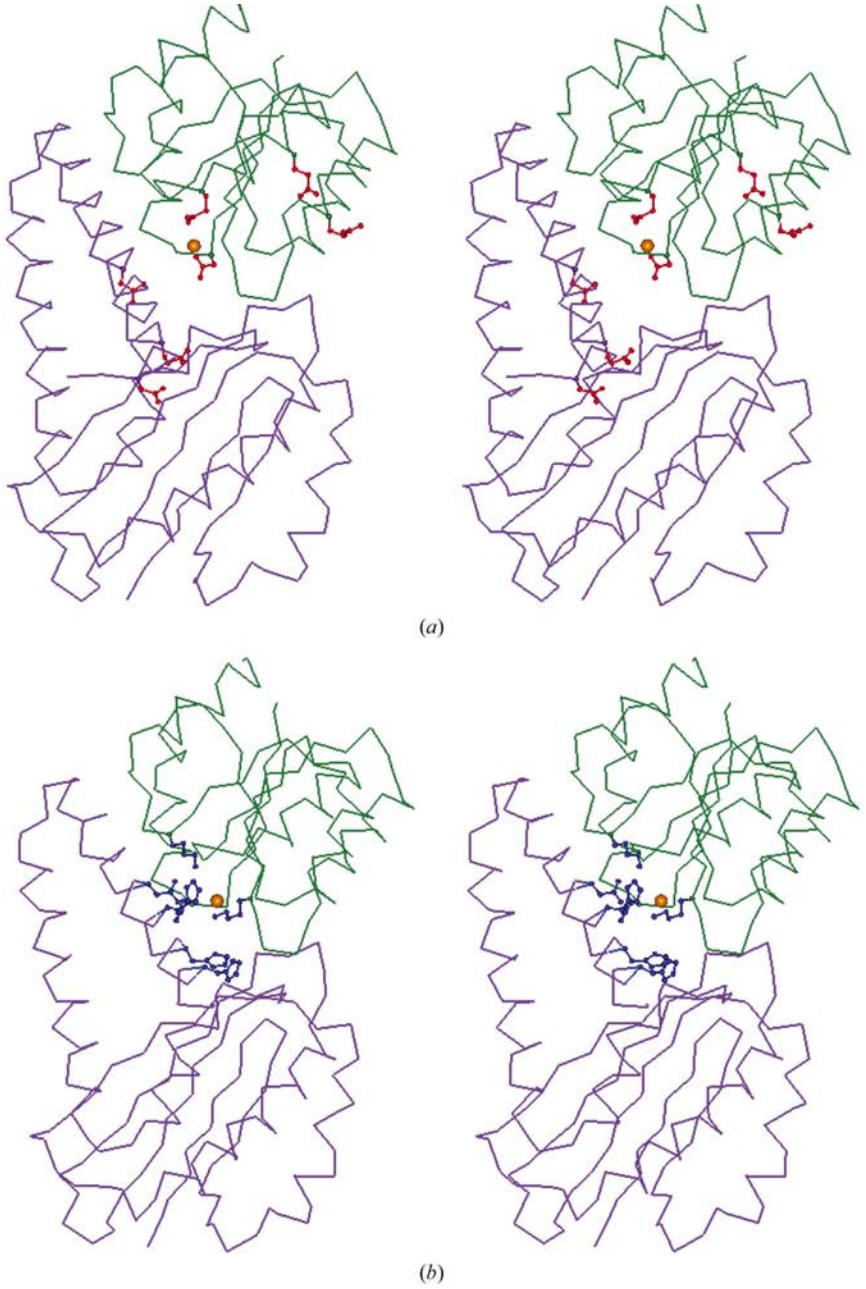

Figure 4
(*a*) A stereoview from above of the channel in the Spo0F–Spo0B complex with acidic groups at the mouth. The Spo0B monomer is colored purple and the two helices of the helix bundle can be seen at the top left-hand corner. The Spo0F monomer is shown in green. The manganese ion at the center is colored orange. (*b*) A similar view of the model where the N-containing side chains along the pocket are shown.

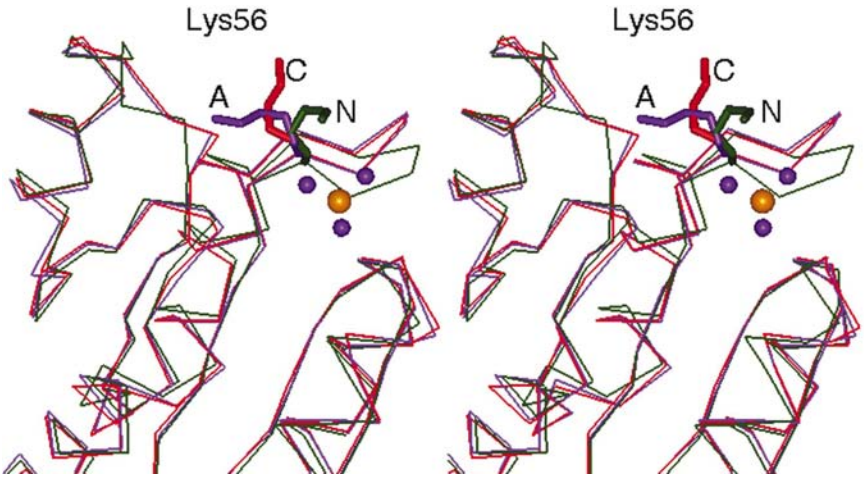

Figure 5
A superposition of three molecules, the native model (green, marked N), Spo0F–Mn^{2+} molecule *A* (purple, marked A) and Spo0F–Mn^{2+} molecule *C* (red, marked C) showing the differing conformations of the Lys56 side chain in the native and metal-bound forms as the side chains move away from the metal center (from N to C and A). Manganese (orange) and three coordinating waters (purple) are taken from the *A* chain.

snapshots along the conformational pathway leading to metal binding. Complex formation of Spo0F and Spo0B creates a favorable microenvironment at the catalytic interface for metal binding, where even the low-affinity cation Mg^{2+} could bind and catalyze phosphotransfer. Manganese is known to act as an activator in metalloproteins, including phosphatases (Reiter *et al.*, 2002). In *B. subtilis*, initiation of sporulation generally takes place when Mn^{2+} is allowed to rise to a sufficient concentration (Inaoka *et al.*, 1999). Using Mn^{2+} instead of Mg^{2+} thus offers another level of biological control in the complex circuitry of sporulation. Further, the observation that Mn^{2+} is essential for sporulation and the current presumptions regarding higher binding of Mn^{2+} at the catalytic pocket suggest manganese has potential therapeutic value for designing an inhibitor containing Mn^{2+} which could act as a pilot to direct the drug to the target.

This work was supported by grant GM54246 from National Institutes of General Medical Sciences, NIH, USPHS.

References

Bellsolell, L., Prieto, J., Serrano, L. & Coll, M. (1994). *J. Mol. Biol.* **238**, 489–495.

Birck, C., Chen, Y., Hulett, F. M. & Samama, J.-P. (2003). *J. Bacteriol.* **185**, 254–261.

Bock, C. W., Katz, A. K., Markham, G. D. & Glusker, J. P. (1999). *J. Am. Chem. Soc.* **121**, 7360–7372.

Brünger, A. T., Adams, P. D., Clore, G. M., DeLano, W. L., Gros, P., Grosse-Kunstleve, R. W., Jiang, J.-S., Kuszewski, J., Nilges, M. & Pannu, N. S. (1998). *Acta Cryst.* D**54**, 905–921.

Burbulys, D., Trach, K. A. & Hoch, J. A. (1991). *Cell*, **64**, 545–552.

Charney, J., Fisher, W. P. & Hegarty, C. P. (1951). *J. Bacteriol.* **62**, 145–148.

Cowan, J. A. (1995). *The Biological Chemistry of Magnesium*, pp. 1–22. New York: VCH.

Dudev, T., Cowan, J. W. & Lim, C. (1999). *J. Am. Chem. Soc.* **121**, 7665–7673.

Dudev, T. & Lim, C. (2001). *J. Phys. Chem. B*, **105**, 4446–4452.

Dudev, T. & Lim, C. (2003). *Chem. Rev.* **103**, 773–788.

Gardino, A. K., Volkman, B. F., Cho, H. S., Lee, S.-Y., Wemmer, D. & Kern, D. (2003). *J. Mol. Biol.* **331**, 245–254.

Gewirth, D. (1994). *The HKL Manual: An Oscillation Data Processing Suite for Macromolecular Crystallography*. Department of Molecular Biophysics and Biochemistry, Yale University. New Haven, CT, USA.

Goudreau, P. N., Lee, P.-J. & Stock, A. M. (1998). *Biochemistry*, **37**, 14575–14584.

Gould, G. W. (1969). *The Bacterial Spore*, edited by G. W. Gould & A. Hurst, pp. 397–444. London: Academic Press.

Grimshaw, C. E., Huang, S., Hanstein, C. G., Strauch, M. A., Burbulys, D., Wang, L., Hoch, J. A. & Whiteley, J. M. (1998). *Biochemistry*, **37**, 1365–1375.

Guillet, V., Ohta, N., Cabantous, S., Newton, A. & Samama, J.-P. (2002). *J. Biol. Chem.* **277**, 42003–42010.

Holm, R. H., Kennepohl, P. & Solomon, E. I. (1996). *Chem. Rev.* **96**, 2239–2314.

Hooft, R. W. W., Vriend, G., Sander, C. & Abola, E. E. (1996). *Nature (London)*, **381**, 272.

Horsburgh, M. J., Wharton, S. J., Karavolos, M. & Foster, S. J. (2002). *Trends Microbiol.* **10**, 496–501.

Im, Y. J., Rho, S.-H., Park, C.-M., Yang, S.-S., Kang, J.-G., Lee, J. L., Song, P.-S. & Eom, S. H. (2002). *Protein Sci.* **11**, 614–624.

Inaoka, T., Matsumura, Y. & Tsuchido, T. (1999). *J. Bacteriol.* **181**, 1939–1943.

Jakubovics, N. S. & Jenkinson, H. F. (2001). *Microbiology*, **147**, 1709–1718.

Jones, T. A., Zou, J.-Y., Cowan, S. W. & Kjeldgaard, M. (1991). *Acta Cryst.* A**47**, 110–119.

Knowles, J. R. (1980). *Annu. Rev. Biochem.* **49**, 877–919.

Laskowski, R. A., MacArthur, M. W., Moss, D. S. & Thornton, J. M. (1993). *J. Appl. Cryst.* **26**, 283–291.

Lee, S.-Y., Cho, H. S., Pelton, J. G., Yan, D., Berry, E. A. & Wemmer, D. E. (2001). *J. Biol. Chem.* **276**, 16425–16431.

Lewis, R. J., Brannigan, J. A., Muchova, K., Barak, I. & Wilkinson, A. J. (1999). *J. Mol. Biol.* **294**, 9–15.

Li, Y. & Plamann, L. (1996). *J. Bacteriol.* **178**, 289–292.

Lukat, G. S., Stock, A. M. & Stock, J. B. (1990). *Biochemistry*, **29**, 5436–5442.

Luzzati, P. V. (1952). *Acta Cryst.* **5**, 802–810.

Madhusudan, Zapf, J. W., Hoch, J. A., Whiteley, J. M., Xuong, N. H. & Varughese, K. I. (1997). *Biochemistry*, **36**, 12739–12745.

Madhusudan, Zapf, J. W., Whiteley, J. M., Hoch, J. A., Xuong, N. H. & Varughese, K. I. (1996). *Structure*, **4**, 679–690.

Matte, A., Tari, L. W. & Delbaere, L. T. J. (1998). *Structure*, **6**, 413–419.

Needham, J. V., Chen, T. Y. & Falke, J. J. (1993). *Biochemistry*, **32**, 3363–3367.

O'Halloran, T. V. (1993). *Science*, **261**, 715–725.

Otwinowski, Z. & Minor, W. (1997). *Methods Enzymol.* **276**, 307–326.

Que, Q. & Helmann, J. D. (2000). *Mol. Microbiol.* **35**, 1454–1468.

Reiter, T. A., Reiter, N. J. & Rusnak, F. (2002). *Biochemistry*, **41**, 15404–15409.

Shan, S. O. & Herschlag, D. (1996). *Proc. Natl Acad. Sci. USA*, **93**, 14474–14479.

Siegbahn, P. E. (2002). *Curr. Opin. Chem. Biol.* **6**, 227–235.

Stock, A. M., Martinez-Hackert, E., Rasmussen, B. F., West, A. H., Stock, J. B., Ringe, D. & Petsko, G. A. (1993). *Biochemistry*, **32**, 13375–13380.

Tari, L. W., Matte, A., Goldie, H. & Delbaere, L. T. (1997). *Nature Struct. Biol.* **4**, 990–994.
Varughese, K. I., Madhusudan, Zhou, X.-Z., Whiteley, J. M. & Hoch, J. A. (1998). *Mol. Cell*, **2**, 485–493.
Yocum, C. F. & Pecoraro, V. L. (1999). *Curr. Opin. Chem. Biol.* **3**, 182–187.
Zapf, J. W., Hoch, J. A. & Whiteley, J. M. (1996). *Biochemistry*, **35**, 2926–2933.
Zapf, J. W., Madhusudan, Grimshaw, C. E., Hoch, J. A., Varughese, K. I. & Whiteley, J. M. (1998). *Biochemistry*, **37**, 7725–7732.
Zapf, J. W., Sen, U., Madhusudan, Hoch, J. A. & Varughese, K. I. (2000). *Structure*, **8**, 851–862.
Zhao, H., Msadek, T., Zapf, J. W., Madhusudan, Hoch, J. A. & Varughese, K. I. (2002). *Structure*, **10**, 1041–1050.